Management and Optimization of a Renewable Energy Hybrid System Integrated into a Microgrid, Considering Constraints Related to Voltage Stability and Service Continuity

R. Mihramane*‡, S. S. Ech-Charqaouy *, D. Saifaoui *, N. Ech-Charqaouy**, A. Ech-Charqaouy **

* Faculty of Sciences of Casablanca AC, Hassan II, University, Casablanca 20100, Morocco

** Physics Laboratory, Faculty of Sciences of Casablanca AC, Hassan II University, Casablanca, Morocco

(redmihramane@gmail.com, echcharqaouy@gmail.com, ddsaifaoui@gmail.com, nizarechcharqaouy@gmail.com, echcharqaouyamjad@gmail.com)

‡ Corresponding Author; R. MIHRAMANE, 20100 Casablanca, Morocco, Tel: 00 212 661 91 07 58,

Fax: 00 212 522 34 05 44, redmihramane@gmail.com

Received: 08.10.2023 Accepted: 24.11.2023

Abstract - This study focuses on optimizing the management of a rural village's microgrid, emphasizing the importance of maintaining the voltage profile. The particle swarm optimization (PSO) algorithm is employed to model the system's behaviour, taking into account various power sources such as wind, photovoltaics, and a diesel generator. Simulations were conducted for a day in July and a day in January, considering variations in weather conditions and demand. The results demonstrate the strategic optimization of the diesel generator to minimize its usage during planned outages while maintaining the voltage profile. Battery storage systems also played a crucial role in maintaining network stability. In conclusion, this study provides a robust methodology and results underscoring the significance of voltage profile maintenance in ensuring reliable energy supply in microgrids.

Keywords: Microgrid, distributed power generation, voltage profile, particle swarm optimization

1. Introduction,

Utilizing renewable energy sources to fulfil energy demands has risen to a top priority in the battle against climate change and in securing a sustainable energy transition. In this regard, microgrids powered by renewable energies have surfaced as a promising solution for effectively and durably meeting local energy demands [1].

A microgrid is considered a local, autonomous, and intelligent energy system. It can be connected to the main electrical grid or operate independently. It can be powered by a variety of energy sources, including renewable energies such as solar, wind, hydropower, and geothermal energy. Microgrids represent one of the optimal solutions to meet the energy needs of a community, building, university or industrial campus, or a specific geographic area [2].

In the last decade, microgrids have been increasingly recognized as flexible, intelligent solutions with great potential for integrating renewable energy sources into the electricity distribution. They are able to improve the reliability, efficiency, and security of the energy system. Furthermore, microgrids can provide better resilience in case of power outages or natural disasters, making them particularly attractive in rural or isolated areas [3].

However, several disadvantages and constraints are associated with renewable energy-powered microgrids. These include:

High construction and installation costs, which can limit their adoption in areas where funding is limited.

Intermittency of renewable energy sources depending on weather conditions and time of day. This intermittency requires sophisticated energy storage technologies to compensate for variations and ensure a constant supply of electricity.

Daily load variations in microgrids can also pose challenges. Microgrids may face fluctuations in electricity demand throughout the day, with demand peaks during peak hours and demand troughs during off-peak hours. Effectively managing these load variations requires flexible and responsive production management strategies [4].

The complexity of managing microgrids is also a challenge. Coordinating and optimizing energy production, load, energy storage, and voltage regulation in a microgrid involves advanced control systems and sophisticated optimization tools. Implementing these systems requires technical expertise and substantial resources.

Production management in microgrids is a fundamental issue that must be fully addressed. It presents increased complexity compared to traditional energy networks, considering the aforementioned elements. It involves coordinating and controlling various energy sources and requires decisions on how to allocate the different sources based on demand, resource availability, and operational constraints.

Furthermore, cost and efficiency optimization are major criteria in this production management within microgrids. Striking a delicate balance between reducing operating costs, maximizing the use of renewable energy sources, and meeting user demand is necessary. This requires the use of advanced optimization tools to make informed decisions while considering the variable system conditions.

Service continuity and voltage plan disruption pose a significant challenge in managing renewable energy production feeding microgrids [5]. Due to the introduction of renewable energies and the decentralization of production, unwanted incidents disrupting power quality can occur, including voltage fluctuations and power outages. These fluctuations may result from variations in renewable energy production depending on weather conditions, variations in demand, or disruptions in the network. As for outages, they can be due to erratic operations resulting from the integration of intermittent renewable energies into the grid or operational issues.

Voltage plan disruption can have several undesirable consequences. Excessive voltage can damage electrical devices and reduce their lifespan, while too low a voltage can lead to inefficient operation of electrical equipment. Moreover, excessive voltage fluctuations can cause disruptions in the network, even power outages [6].

In microgrid management, voltage plan disruption and production management are closely related issues. Voltage fluctuations can be exacerbated by variations in renewable energy production, making production management even more crucial to maintain system stability [7].

2. Problem Statement

In summary, we face a central issue that lies in finding effective solutions to optimize the use of multiple sources powering the microgrid while ensuring stability, reliability, and efficiency of the microgrid. Balancing costs, resource availability, and user satisfaction is crucial.

3. Proposed Solution

To address this challenge of managing renewable energy production in a microgrid while aiming to mitigate issues related to voltage plan disruption, we adopt a strategy that focuses on optimizing the use in an intelligent and efficient manner, aiming to maximize benefits (minimizing costs) and improve competitiveness. For this purpose, we considered a specific economic model that takes into account operating costs based on various parameters and electrical indicators, including active and reactive electrical powers. This model is discrete and nonlinear, leading us to utilize metaheuristic optimization tools to minimize operating costs [8].

Indeed, we have chosen a specific algorithm to determine the cost and emission functions, considering the energy demand of consumers. We have also introduced an automatic voltage regulation device to maintain the voltage plan and keep fluctuations at their minimal values in all microgrid nodes.

The ultimate goal of optimizing our proposed management system is to determine the appropriate parameters of a function to minimize or maximize its value while respecting specific constraints. However, it's not just about finding the most suitable solution for our problem; it's also about ensuring that this solution is feasible and aligns with the inherent characteristics of this problem [9].

Among the evolution-based optimization methods, we have opted for one of the most effective ones, the Particle Swarm Optimization (PSO) algorithm. This algorithm has seen extensive adoption in multi-objective problems due to its population-based search capability, simplicity, rapid convergence, and robustness. The origin of PSO dates back to its first introduction by Kennedy and Eberhart [10], drawing inspiration from observed social behaviours in animals, using concepts from computer graphics and social psychology.

In general, PSO simulates interactions within a group of birds called a "swarm," where each feasible solution is represented by a bird, referred to as a "particle." Each particle has its own objective function value (or fitness function) denoted as f and possesses a velocity vector governing its movement within the search space [11]. To converge to the optimal point, particles update their future trajectories based on their current velocities, their individual best performances, and the best performances observed by their most successful

informants, as illustrated in Figure 1 and formulated as follows [12]:

The velocity of movement V_{ij}^{k+1} of a particle i from position X_i^k to position X_i^{k+1} in the search space, along dimension j, considering its last movement velocity was V_{ij}^k, is given by equation (1).

$$V_{ij}^{k+1} = \omega_i V_{ij}^k + C_1 Rand1(.)\left(P_{Xbestij}^k - X_{ij}^k\right) + C_2 Rand2(.)\left(P_{Gbestj}^k - X_{ij}^k\right) \quad (1)$$

The new position taken by particle i in its (k+1) th movement along dimension j, given that it was at position X_{ij}^k along the same dimension, is given by equation (2):

$$X_{ij}^{k+1} = X_{ij}^k + V_{ij}^{k+1} \quad (2)$$

Where $P_{Xbestij}^k$ represents the position recorded as the best position occupied by particle i since the beginning of the search until its k-th movement, P_{Gbestj}^k denotes the position recorded as the best position occupied by the best particle in the swarm (informant particle) since the beginning of the search until their k-th movement, the notations Rand(.) 1 and 2 denote two random numbers in the range [0,1], the letters C_1 and C_2 represent the learning or acceleration factors. As for ω_i, it corresponds to the inertia weight factor associated with particle i

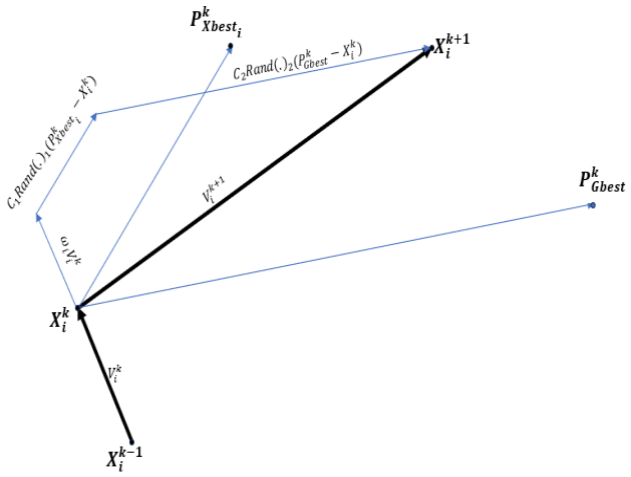

Fig. 1. Geometric construction of PSO parameters.

The variables PXbest and PGbest, along with their adjustments, are both crucial. Conceptually, PXbest can be likened to autobiographical memory, as each individual remembers their personal experience (even if it's just an aspect of it), and the velocity adjustment associated with PXbest can be described as a form of "simple nostalgia." Indeed, the individual tends to return to the place that brought them the most satisfaction in the past. On the other hand, PGbest, can be seen as a form of shared knowledge, a group norm, or a goal that individuals collectively strive to achieve [13].

The objective function f, also known as the fitness function, is a continuous or discrete mathematical function from Rn to R that needs to be minimized (or maximized) in the context of the Particle Swarm Optimization (PSO) problem. It quantifies the performance, quality, or value of a candidate solution in the problem's context.

In iteration k+1, the variable P_{Xbest} is determined as follows:

$$P_{Xbestij}^{k+1} = X_{ij}^{k+1} \text{Si } f(X_{ij}^{k+1}) \leq f(P_{Xbestij}^k) \quad (3)$$

$$P_{Xbestij}^{k+1} = P_{Xbestij}^k \text{ Si } f(X_{ij}^{k+1}) > f(P_{Xbestij}^k) \quad (4)$$

As for the position P_{Gbest}, it is determined within the same iteration k+1 by:

$$P_{Gbestj}^{k+1} = X_{ij}^{k+1} \text{ Si } f(X_{ij}^{k+1}) \leq f(P_{Gbestj}^k) \quad (5)$$

$$P_{Gbestj}^{k+1} = P_{Gbestj}^k \text{ Si } f\left(X_{ij}^{k+1}\right) > f(P_{Gbestj}^k) \quad (6)$$

4. Problem Formulation

The objective of the optimization function in our proposed management system is to find optimal operating points in terms of power for dispersed electricity generators (DGs), electricity storage systems by batteries (BSSs), and the main grid, considering economic, environmental, and voltage stability constraints.

4.1. Cost Minimization

Developing a cost function is a crucial step in the efficient design and management of micro-grids. This function is fundamentally important as it determines how the energy resources of the micro-grid are utilized to meet load requirements while minimizing associated costs.

However, it is inherent in this context that the objective is always to minimize the overall system costs as well as the pollutant emissions. Moreover, ensuring electricity demand is met is essential. This consideration is even more crucial given that the micro-grid can operate either connected to the electricity grid or in an autonomous mode.

To elaborate further, in the context of autonomous mode, it is imperative to minimize the overall system cost, fuel emissions, and the probability of not meeting the electricity demand. Regarding the grid-connected mode, the objective remains to minimize the overall system cost, fuel emissions, and the share of non-renewable energy.

Various functions have been used in different studies. According to Amoura et al. [14], in some studies, the operating cost of decentralized resources and the storage system was considered constant throughout the day, while the selling/buying prices from the main grid varied. In other studies, the cost of decentralized resources and the storage system was considered dynamic throughout the day.

In the case of Morocco, the current regulations have not yet set the selling prices of kWh to the utility. We consider these two prices to be the same and fixed throughout the day. Given that the operating costs of DGs and BSSs are calculated based on average prices of raw materials, materials, and

services implemented, we consider these costs to be fixed during the day.

- Cost Function

This function can be expressed as follows:

$$f_{coût}(x) = \sum_{t=1}^{T}\{[\sum_{i=1}^{M_{DG}}(S_i(t)P_{DG_i}(t)C_{DG_i}(t) + SC_{DG_i}(t)|S_i(t) - S_i(t+1)|)] + [\sum_{j=1}^{M_{BES}}(S_j(t)\,P_{BES_j}(t)C_{BES_j}(t) + SC_{BES_j}(t)|S_j(t) - S_j(t+1)|)] - P_{in}(t)C_{in}(t) + P_{dr}(t)C_{dr}(t)\} \quad (7)$$

here t represents time in hours (h) and T is the total number of hours in a day. Similarly, at time t, in equation (7), P_{DGi} (t) symbolizes the active power in kilowatts (kW) actually supplied at that hour by the distributed electricity generation (DG_i), M_{DG} represents the total number of DGs in the microgrid P_{BSSj} (t) represents the charging or discharging power in kilowatts (kW) of the battery energy storage system (BSS_j). M_{BSS} corresponds to the total number of BSSs in the microgrid. $S_i(t)$ embodies the state of distributed resource i (ON = 1/OFF = 0), while $S_j(t)$ represents the state of BSS_j (ON = 1/OFF = 0). $P_{in}(t)$and $P_{dr}(t)$ represent respectively the active power injected into the main grid and the active power drawn from it in kilowatts (kW). $C_{DGi}(t)$ denotes the total cost of kilowatt-hour produced by the distributed generation DG_i, expressed in Moroccan Dirham (MDH), $C_{BSSj}(t)$ corresponds to the total operating cost of the storage element, expressed in Moroccan Dirham per kilowatt-hour (MDH/kWh), $C_{dr}(t)$ represents the cost of purchasing energy from the main grid, expressed in Moroccan Dirham per kilowatt-hour (MDH / kWh, $C_{in}(t)$ represents the cost of selling energy to the grid, expressed in Moroccan Dirham per kilowatt-hour (MDH/kWh), $SC_{DGi}(t)$ and $SC_{BSSj}(t)$ represent respectively the start-up or shut-down costs of distributed resources DG_i and BSS_j, expressed in Moroccan Dirham (MDH). As specified above, $C_{dr}(t)= C_{in}(t)=C_u$. C_u is constant over the period [1, T], so equation (7) can be written as follows:

$$f_{coût}(x) = \sum_{t=1}^{T}\{[\sum_{i=1}^{M_{DG}}(S_i(t)P_{DG_i}(t)C_{DG_i}(t) + SC_{DG_i}(t)|S_i(t) - S_i(t+1)|)] + [\sum_{j=1}^{M_{BES}}(S_j(t)\,P_{BES_j}(t)C_{BES_j}(t) + SC_{BES_j}(t)|S_j(t) - S_j(t+1)|)] + (P_{dr}(t) - P_{in}(t))C_u\} \quad (8)$$

Where C_u represents the selling cost of the energy supplied to the main grid and the purchasing cost of the energy imported from the grid [15].

- Emission Function

In the context of our study, it is important to consider the production means that emit greenhouse gases (GHGs) in addition to those associated with energy supplied by the public grid. Among these sources, we identify Stationary Storage Batteries (BSS) as well as diesel generators (DG). The latter represent substantial sources of emissions of these harmful gases to the environment.

The predominant emissions related to these diesel generators mainly result from the combustion of diesel, a process that releases carbon dioxide (CO2), carbon monoxide (CO), as well as nitrogen oxides (NOx) into the atmosphere. CO2 deserves particular attention as it is a major greenhouse gas responsible for climate change. CO2 emissions are directly correlated with the amount of diesel fuel burned, so prolonged use of these diesel generators, especially at low loads, can have a substantial impact on the total CO2 emissions [16]. This is how the emission function is expressed as follows:

$$f_{emission}(x) = \sum_{t=1}^{T}\{[\sum_{i=1}^{M_{DG}}(S_i(t)P_{DG_i}(t)E_{DG_i}(t)] + [\sum_{j=1}^{M_{BES}}(S_j(t)\,P_{BSS_j}(t)E_{BSS_j}(t)] - P_{in}(t)E_{in}(t) + P_{dr}(t)E_{dr}(t)\} \quad (9)$$

At time t, in equation (9), $E_{DGi}(t)$ embodies the greenhouse gas emission rate associated with the energy produced by DG_i, expressed in grams per hour per kilowatt (g/(h kW)), $E_{BSSj}(t)$ corresponds to the greenhouse gas emission rate associated with the energy supplied/absorbed by the storage element BSS_j, expressed in grams per hour per kilowatt (g/(h kW)), $E_{dr}(t)$ represents the greenhouse gas emission rate associated with the energy imported from the main grid, expressed in grams per hour per kilowatt (g/(h kW)), while $E_{in}(t)$ represents the greenhouse gas emission rate associated with the energy exported to the main grid, expressed in grams per hour per kilowatt (g/(h kW)).

In the context of this study, which presents increased complexity due to constraints related to voltage stability, we decide to simplify the bi-objective problem. Our method aims to convert this bi-objective problem into a mono-objective problem by integrating linearly, into the initial cost, a penalty or tax associated with greenhouse gas emissions into the environment.

The cost of this penalty for emitting one ton of greenhouse gases (GHGs) into the environment, also called the carbon price, varies considerably depending on various parameters such as the country, the carbon market, government policies, and the nature of the emitted GHGs. In some regions of the world, there are carbon markets where companies must acquire carbon credits to offset their excess emissions. The price of these carbon credits can vary based on supply and demand in the market.

Currently, Morocco has not established a specific tax on greenhouse gas (GHG) emissions at the national level. However, the country has implemented various initiatives and policies aimed at reducing these emissions and encouraging the transition to cleaner energy sources. A bill is also underway to penalize environmental pollution due to GHGs.

To establish a reasonable unit cost of the tax to apply in our study, we adopted the French legislation in this context. In France, this tax is currently set at approximately €22 per tonne of CO2 emitted during the production of a product or service.

The French government has set a goal for this tax to reach 100 euros per tonne of CO2 by 2030, an amount established in the Energy Transition Law of August 2015 [17].

. So, we propose a new objective function that will be considered for the remainder of this study, as follows

$$f_{coût}(x) = \sum_{t=1}^{T}\{[\sum_{i=1}^{M_{DG}}(S_i(t)P_{DG_i}(t)C_{DG_i}(t) + SC_{DG_i}(t)|S_i(t) - S_i(t+1)|)] + [\sum_{j=1}^{M_{BES}}(S_j(t)\,P_{BES_j}(t)C_{BES_j}(t) + SC_{BES_j}(t)|S_j(t) - S_j(t+1)|)] + (P_{dr}(t) - P_{in}(t))C_u + [\sum_{i=1}^{M_{RDG}}(S_i(t)P_{DG_i}(t)E_{DG_i}(t)CE_{DG_i}(t)] + [\sum_{j=1}^{M_{BES}}(S_j(t)\,P_{BSS_j}(t)E_{BSS_j}(t)CE_{BSS_j}(t)] - P_{in}(t)E_{in}(t)CE_{in} + P_{dr}(t)E_{dr}(t)CE_{dr}\} \quad (10)$$

In equation (10) at time t, $CE_{DGi}(t)$ embodies the greenhouse gas emission tax cost related to the energy produced by DG_i, expressed in (MDH/grams). $CE_{BSSj}(t)$ corresponds to the greenhouse gas emission tax cost associated with the energy supplied/absorbed by the storage element BSSj, expressed in (MDH/grams). $CE_{dr}(t)$ represents the greenhouse gas emission tax cost related to the energy imported from the main grid, expressed in (MDH/grams), while $CE_{in}(t)$ represents the greenhouse gas emission tax cost associated with the energy exported to the main grid, in (MDH/grams).

4.2. Constraints Associated with Micro-Grid Operation

4.2.1. Balance of supplied and demanded power

To ensure the electrical stability of the micro-grid, the electrical power absorbed by the loads must be equal to that provided by the generation systems. Formula (11) expresses this condition.

$$\sum_{k=1}^{N_c} P_{ck} = \sum_{t=1}^{T}\{[\sum_{i=1}^{M_{RDG}}(S_i(t)P_{RDG_i}(t)+)] + [\sum_{j=1}^{M_{BES}}(S_j(t)\,P_{BES_j}(t))] - P_{in}(t) + P_{dr}(t)\} \quad (11)$$

Where $Pc_k(t)$ represents the power (kW) demanded by customer k, and N_c represents the total number of customers in the microgrid.

4.2.2. Actual energy production capacity

For stable operation, the active power production of each DG is limited by lower and upper bounds as follows:

For proper operational conditions, the actively supplied powers by the various DGs must adhere to the following inequalities:

$$P_{DGi}^{min}(t) \le P_{DGi}(t) \le P_{DGi}^{max}(t) \quad (12)$$

$$P_{BSSj}^{min}(t) \le P_{BSSj}(t) \le P_{BSSj}^{max}(t) \quad (13)$$

$$0 \le P_{in}(t) \le P_{in}^{max}(t) \quad (14)$$

In equations (12), (13), and (14), at time t, $P_{DGi}^{min}(t)$ and $P_{DGi}^{max}(t)$ represent the minimum and maximum power output that DGi can generate. $P_{BSSj}^{min}(t)$ and $P_{BSSj}^{max}(t)$ denote the minimum power that BSS_j can produce, and $P_{in}^{max}(t)$ embodies the maximum power injected into the main grid.

4.2.3. Voltage profile maintenance constraints

Here, we refer to the work of ECH-CHARQAOUY et al. [6] who developed a nodal topology-based model to determine the voltage profile in an electrical line by calculating the voltage value at each of its nodes, as shown in Fig. 2.

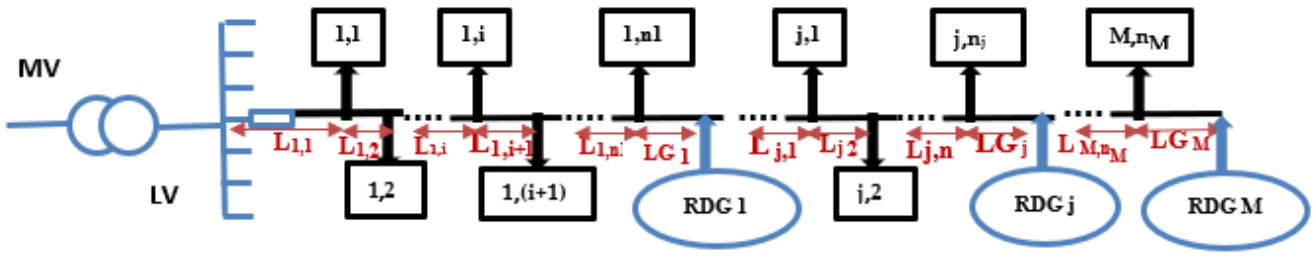

Fig. 2. Simplified line diagram with different nodes: connection points for clients and DGs.

In this formulation, n1 denotes the number of clients connected upstream of the junction point with Distributed Generation of electricity (DG1), nj represents the number of clients connected between the interconnection points of DGj-1 and DGj, while nM-1 represents the number of clients connected between the interconnection points of DGM-2 and DGM-1. The parameter nM designates the number of clients connected between the interconnection point of DGM-1 and the end of the network (assuming that in the absence of Renewable Distributed Generation at this end, a fictitious DGM with zero production is present). The symbol N represents the total consumers within the microgrid, while M refers to the number of Renewable Distributed Generators. The notation (j,i) refers to the connection point of client i, located between DGj-1 and DGj; The quantities Lji and LGj represent the lengths of line segments between the connection

point (j,(i-1)) and the connection point (j,i), and between the connection point (j,nj) and the connection point of DGj. Additionally, Pji symbolizes the value of active power at the connection point (j, i) in watts, PGj denotes the value of active power of DGj in watts, Qji corresponds to the value of reactive power of DGj in volt-amperes reactive (VAR), and QGj represents the value of reactive power of DGj, also in volt-amperes reactive (VAR):

$$N = \sum_{j=1}^{j=M} n_j \quad (15)$$

Where :

The voltage drops in a line segment of length L in (m), linear resistance r in (Ω), and linear reactance x in (Ω), feeding an electrical receiver with active power P in (W) and reactive power Q in (VAR), under a voltage U in (V), is given by the formula: [18]

$$\Delta U = \frac{L}{U}(rP + xQ) \quad (16)$$

By applying this formula to different nodes along the electrical line, the following general equations can be obtained [6]:

$$\Delta Ufk = \frac{L_{fk}}{(U_{f(k-1)})}\left(r\left[\sum_{i=k}^{nf} P_{fi} + \sum_{j=f+1}^{M}\sum_{i=1}^{nj} P_{ji} - \sum_{j=f}^{M} PGj\right] + x\left[\sum_{i=k}^{nf} Q_{fi} + \sum_{j=f+1}^{M}\sum_{i=1}^{nj} Qji - \sum_{j=f}^{M} QGj\right]\right) \quad (17)$$

$$\Delta UG_f = \frac{Lf}{(U_{f n_f})}\left(r\left[\sum_{j=f+1}^{M}\sum_{i=1}^{nj} P_{ji} - \sum_{j=f}^{M} PG_j\right] + x\left[\sum_{j=f+1}^{M}\sum_{i=1}^{nj} Q_{ji} - \sum_{j=f}^{M} QG_j\right]\right) \quad (18)$$

$$S\Delta U_{fk} = \left(\sum_{j=1}^{f-1}\sum_{i=1}^{nj} \Delta U_{ji} + \sum_{i=1}^{k} U_{fi} + \sum_{j=1}^{f-1} \Delta UG_j\right) \quad (19)$$

$$S\Delta U_{Gf} = (S\Delta U_{f n_f} + \Delta UG_f) \quad (20)$$

$$U_{fk} = (U_S - S\Delta U_{fk}) \quad (21)$$

$$UG_f = (U_S - S\Delta UG_f) \quad (22)$$

In this formulation, U_s denotes the voltage value at the output of the link transformer between the microgrid and the main grid, while U_{ji} represents the voltage value at node (j, i). UG_j indicates the voltage value at the connection point of DG_j, and ΔU_{ji} refers to the voltage drop value between node (j, i-1) and node (j, i). Similarly, ΔU_{Gj} represents the voltage drop value between node (j, n_j) and the connection point of DG_j. $S\Delta U_{ji}$ symbolizes the sum of voltage drops between node (1,1) and node (j,i), and $S\Delta U_{Gj}$ expresses the sum of voltage drops between node (1,1) and the connection point of DG_j. The parameters r and x represent the linear resistance and linear reactance, respectively, expressed in Ohms (Ω).

Taking into account the permissible voltage drops according to the applicable standards in Morocco, which is 10%, we can write the inequalities representing the maintenance of the voltage profile as follows:

$$U_S - 10\% \le U_{fk} = (U_S - S\Delta U_{fk}) \le U_S + 10\% \quad (23)$$

$$U_S - 10\% \le U_{Gf} = (U_S - S\Delta U_{Gf}) \le U_S + 10\% \quad (24)$$

This can be simplified as follows:

$$-10\% \le (S\Delta U_{fk}) \le 10\% \quad (25)$$

$$-10\% \le (S\Delta UG_f) \le 10\% \quad (26)$$

4.2.4. Constraints on charging and discharging operations of electrical energy storage batteries

Electrical energy storage batteries are essential components in the field of renewable energy and electricity management. They allow for storing surplus electrical energy for later use, contributing to optimizing energy consumption and stability of electrical grids. The charging and discharging operations of batteries are governed by fundamental principles and quantitative equations.

During the charging operation, electricity from an external power source is converted into chemical energy and stored in the battery. The important parameters in this operation are the battery charging power at a time t, $P_{charge}(t)$ (in watts), the time interval considered, Δt (in seconds), and the charging efficiency of the battery, η_c. The quantitative formula for battery charging is as follows:

$$E(t+1) = E(t) + \Delta t\, P_{charge}(t)\, \eta_c \quad (27)$$

On the other hand, during the discharging operation, the energy stored in the battery is converted into electricity to power devices or electrical systems. The important parameters during discharge are the battery discharge power at a time t, $P_{discharge}(t)$ (in watts), the time interval considered, Δt (in seconds), and the discharging efficiency of the battery, η_d. The quantitative formula for battery discharging is as follows:

$$E(t+1) = E(t) - \Delta t \frac{P_{discharge}(t)}{\eta_d} \quad (28)$$

Where E(t) is the energy stored in the battery at time t (in joules) in both operations.

These quantitative equations describe the charging and discharging processes of electrical energy storage batteries and can be replaced by a single formula as follows:

$$E(t+1) = E(t) + \Delta t P_{discharge}(t)\eta_c - \Delta t \frac{P_{discharge}(t)}{\eta_d} \quad (29)$$

Power Constraints for Battery Charging: During these charge and discharge operations of a battery, there are typically constraints on the maximum allowed charging power and maximum allowed discharging power. These constraints are in place to preserve the battery and ensure its safe and optimal operation [19]. These constraints are expressed as follows:

$$P_{Chargemax}(t) = N_{bat} \min\left(0, \frac{V_{bat}(SOC_{max} - SOC(t))C_{bat}}{\Delta t}\right) \quad (30)$$

$$P_{Dischargemax}(t) = N_{bat} \min\left(0, \frac{V_{bat}(SOC(t) - SOC_{min})C_{bat}}{\Delta t}\right) \quad (31)$$

In this equation, $P_{charge\_max}(t)$ represents the maximum charging power of the battery at time t, expressed in watts. Similarly, $P_{discharge\_max}(t)$ represents the maximum discharging power of the battery at time t, also in watts. The term N_{bat} refers to the number of batteries, whether arranged in series or parallel. V_{bat} symbolizes the nominal voltage of each battery, expressed in volts. Additionally, SOC(t) represents the current state of charge of the battery at time t, expressed in decimals. The parameters SOC_{max} and SOC_{min} define the maximum and minimum allowable state of charge for the battery, still in decimals. The quantity C_{bat} corresponds to the nominal capacity of each battery, measured in ampere-hours, while Δt represents the considered time interval, expressed in seconds.

These constraints ensure that the power never exceeds the battery's charging capacity or pushes it beyond its maximum charge limit. These constraints ensure that the charging and discharging powers do not exceed the battery's charging and discharging capacities, respectively.

5. Simulation Methodology and Algorithm Parameters

5.1. Simulation Methodology

To assess the relevance and robustness of our proposed approach, we conducted a simulation on a representative microgrid system, characterized as follows: The microgrid serves a rural village comprising 218 households, each with an average power demand of 600 W, alongside three commercial entities consuming 1 kW each, and two electric motors rated at 15 kW and 20 kW, respectively. The primary low-voltage (LV) distribution line spans 2,170 meters and consists of twisted aluminum conductors with a cross-sectional area of 70 mm². This network is connected to the main utility grid via a prefabricated medium-to-low voltage (MV/LV) masonry substation. The substation is equipped with a 250 kVA transformer, two motorized MV switchgear cells, a fuse-protected transformer cell, a bidirectional smart LV meter, and a distribution board featuring a main circuit breaker and two LV feeders, each protected by a motorized circuit breaker.

Furthermore, this micro-grid is also powered by a wind turbine with a capacity of 90 kW, a photovoltaic plant of 44 kW, and a 50 kVA diesel generator. Among its customers are two energy producers with photovoltaic plants of 10 kW and 6 kW, respectively. The diagrams in Fig. 3 provide more details about this micro-grid.

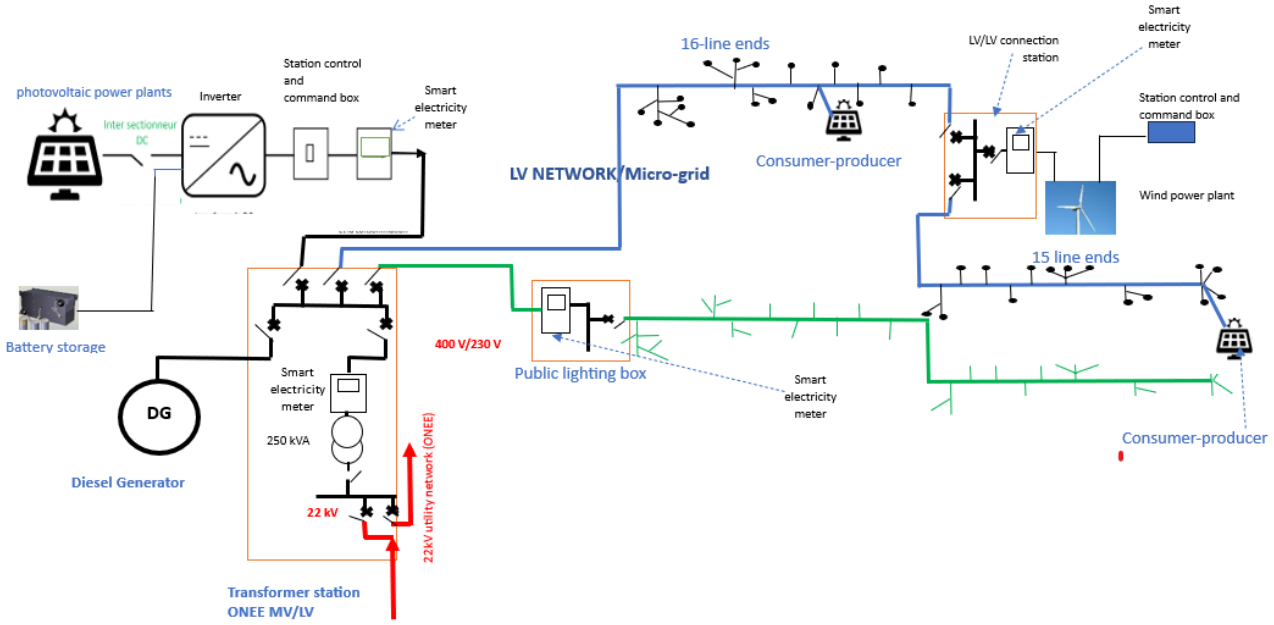

Fig. 3. Electrical diagram of the studied microgrid.

As previously mentioned, this microgrid is equipped with nine power sources, namely a main photovoltaic power station, two small photovoltaic stations owned by client-producers, three electricity storage systems by batteries, each associated with a photovoltaic power station, a wind turbine, and a diesel generator. It is worth noting that the main grid can supply or absorb electrical energy from the microgrid. In this regard, the decision variables are ($P_{DG^1}(t)$, $P_{DG^2}(t)$, $P_{DG^3}(t)$, $P_{DG^4}(t)$, $P_{DG^5}(t)$, ($P_{in}(t)$ or $P_{dr}(t)$), $P_{BSS^2}(t)$, $P_{BSS^3}(t)$, $P_{BSS^5}(t)$).

Where $P_{DG1}(t)$ represents the power supplied by the diesel generator, $P_{DG2}(t)$ the power supplied by the main photovoltaic power station, $P_{DG3}(t)$ the power supplied by the photovoltaic

power station of the first client-producer, $P_{DG4}(t)$ the power supplied by the wind turbine (WT), $P_{DG5}(t)$ the power supplied by the photovoltaic power station of the second client-producer, $P_{in}(t)$ and $P_{dr}(t)$ respectively represent the active power injected into the main grid and the active power drawn from it, $P_{BSS2}(t)$ represents the power of the battery storage system associated with the main photovoltaic power station, $P_{BSS3}(t)$ represents the power of the battery storage system associated with the photovoltaic power station of the first client-producer, and $P_{BSS5}(t)$ represents the power of the battery storage system associated with the photovoltaic power station of the second client-producer.

The simulation will cover the 24 hours of a day in July 2023, chosen as the reference. This simulation will be carried out with an hourly time interval. The performance of the production sources is detailed as follows:

- Wind turbine

The wind turbine consists of a single turbine with a nominal power of 45 kW. It generates an average of 90 MWh of electrical energy at an average wind speed of 5 m/s.

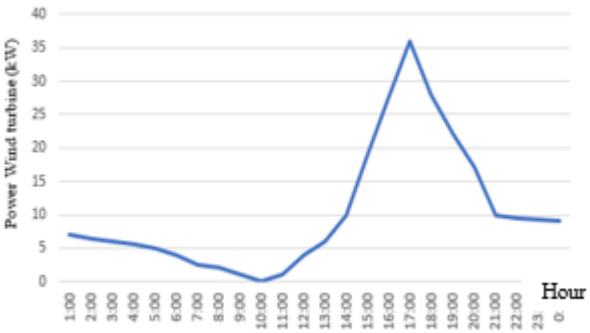

Fig. 4. The electrical power in (kW) provided by the wind turbine during a day (24 hours).

Figure 4 depicts the variation in electrical power supplied by the wind turbine over a 24-hour period during a summer day. It is noteworthy that the maximum power supplied by this wind turbine is 36 kW around 5:00 PM. Additionally, it should be noted that the turbine can deliver virtually no power between 9:00 AM and 11:00 AM.

- PV Power Plants

Three curves illustrate the variation in power produced in watts by the main PV power plant, with a total peak power of 44 kWp, over three different days of the year. These data are depicted in the numbered figures. As indicated in the figure 5, the maximum power produced by the PV power plant varies approximately between 10 kW and 44 kW depending on the days of the year. This power will be calculated using the optimization algorithm employing a predictive algorithm for the maximum power of a PV power plant, developed in our previous work.

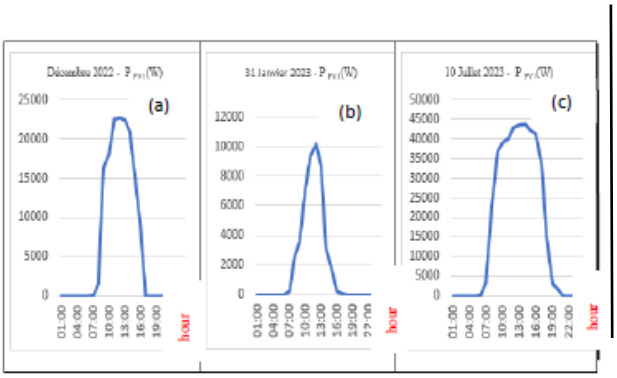

Fig. 5. (a) - The electrical power in kilowatts supplied by the photovoltaic power station during the hours of the day on Decembre 10, 2022. (b) - The electrical power in kilowatts supplied by the photovoltaic power station during the hours of the day on January 31, 2023. (c) - The electrical power in kilowatts supplied by the photovoltaic power station during the hours of the day on Jully 10, 2023.

- Diesel Generator

To ensure proper functioning of the diesel generator, preserving its reliability and lifespan, the delivered power must be maintained between 30% and 70% of its nominal power

Table 2. Maximum and minimum limit of the power generated by the diesel generator.

Minimum power supplied by the diesel generator (kW)	Maximum power supplied by the diesel generator (kW)
15	35

- Battery Storage Systems

To maximize the lifespan of the electrical storage batteries, it is essential to tailor the percentage state of charge (SOC) levels to each battery's unique characteristics, including its technology, design, and specific usage. In the case of batteries used in conjunction with the three photovoltaic (PV) power plants, all of which are lead-acid type, it was determined that the maximum state of charge (SOC_{max}) would be set at 90%, while the minimum state of charge (SOC_{min}) would be established at 40%, to preserve their longevity and efficiency.

- Load Profile

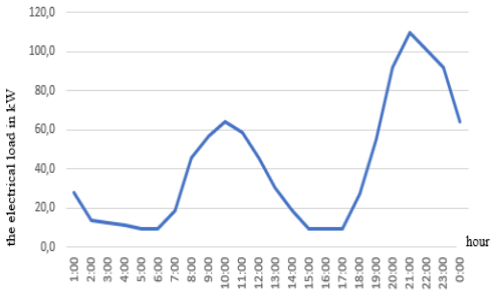

Fig. 6. the electrical load in kW.

Figure 6 highlights the daily load profile required by the microgrid consumers over the course of 24 hours on a summer day. This representation reveals two daily peaks, with a modest peak of 64 kW recorded around 10:00 AM, followed by a larger peak of 110 kW around 9:00 PM.

5.2. Parameterization of the Algorithm

The use of the Particle Swarm Optimization (PSO) algorithm requires a careful selection of parameters in formula (1), namely ωi, c1, and c2, as well as determining the population size and the maximum number of iterations.

In our case, we chose a population size equivalent to 6 times the number of variables, i.e., 54 individuals, and a maximum number of iterations of 1000. The algorithm was implemented in the MATLAB environment.

As expressed by formula (1), the inertia coefficient, represented by ω, has a decisive influence on the future trajectory the particle will follow in its movement. It is a crucial parameter that balances global-scale exploration and local-scale exploitation judiciously, thus providing adequate optimization to the conducted search. The extent of exploration in the search space significantly depends on the value assigned to the inertia weight. A high value of this parameter favours extensive exploration on a global scale, whereas a more modest value promotes targeted exploration on a local scale [20].

In his thesis, Frans van den Bergh [21] confirmed that optimal performance was achieved by adjusting the inertia weight from 0.9 to 0.4 during the first 1500 iterations. Furthermore, it is common in specialized literature for this inertia coefficient to undergo a temporal evolution over the iterations. This evolution is generally linear, starting at 0.9 and eventually reaching 0.4, as described by Shi [22]. The inertia coefficient, symbolized by ω, thus undergoes variations over time, following the formula [23]:

$$\omega = \omega_{max} - \frac{(\omega_{max} - \omega_{min})}{N_{iteration\ max}} N_{iter} \qquad (32)$$

Where $\omega_{min} = 0.4$, $\omega_{max} = 0.9$, $N_{iteration\_max} = 1000$, and N_{iter} represents the current iteration number.

The trust factors influence the particle's inclinations to follow either its preservation instinct or the group's guidance. The random variables c1rand() and c2rand() can be defined according to a uniform distribution over the interval [0..1]. The positive constants c1 and c2 are determined empirically, and they must satisfy the relation $c1 + c2 \leq 4$. In this study, we choose $c1 = c2 = 2$.

6. Optimization Results and Discussion

In this section, we present the results of our optimization study using the previously described PSO algorithm. Two scenarios were considered to evaluate the system's performance: the first over a 24-hour period on a Sunday in July, where a scheduled power outage was planned for maintenance; and the second over 24 hours on a day in January during winter.

In the first scenario, the distribution of the contribution from different energy sources is shown in figure 7. Despite the higher cost per kilowatt-hour produced by the diesel generator compared to other sources, it significantly contributed to powering the microgrid. This can be attributed to the unavailability of the main grid between 06:00 and 14:00, during which the diesel generator was engaged.

Fig. 7. PSO results, July 10th – Summer.

As illustrated in Figure 8, the total hourly cost function, incorporating energy prices and greenhouse gas emission taxes, exhibits two peaks. The first peak, reached around 10:00, is due to the operation of the diesel generator between 07:00 and 14:00, when the kilowatt-hour price is high. The second peak, a global maximum for the day, occurs around 21:00, explained by exclusive power supply from the main grid and the peak in load reaching its maximum at this time. The cost function is negative between 13:00 and 18:00 due to the excess production from renewable energy sources, surplus injected into the main grid and sold to the utility.

Fig. 8. Cost function per hour, July 10th – Summer.

Greenhouse gas emissions reach their maximum around 21:00, as presented in figure 9, for the same reasons as the increase in the cost function. Optimization also effectively utilized the energy storage systems (BSSs), which actively contributed to powering the microgrid during the night, between 01:00 and 05:00. During this period, renewable energy source production is at its lowest.

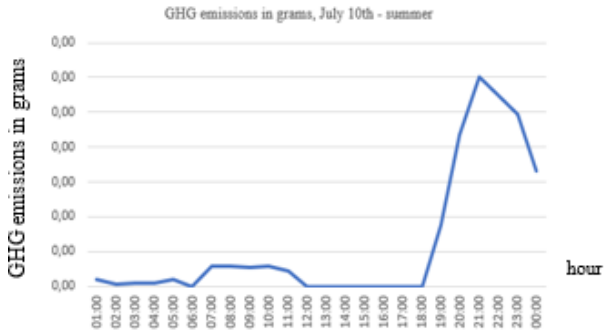

Fig. 9. GHG emissions, July 10th – Summer.

The BSSs were charged as soon as the diesel generator was compelled to start to supply the microgrid due to the unavailability of the main grid and inadequate production from other sources. Charge and discharge curves for the BSSs are depicted in Figures 11, 12, and 13.

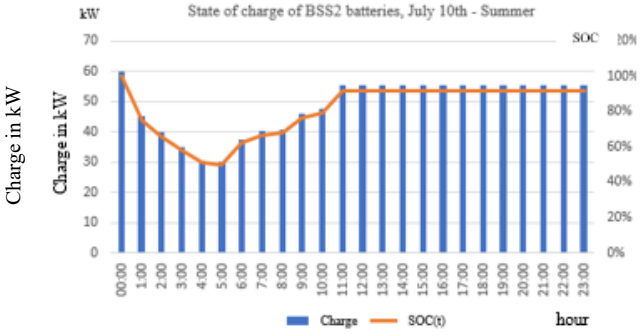

Fig. 10. state of charge of BSS2 batteries, July 10th – Summer.

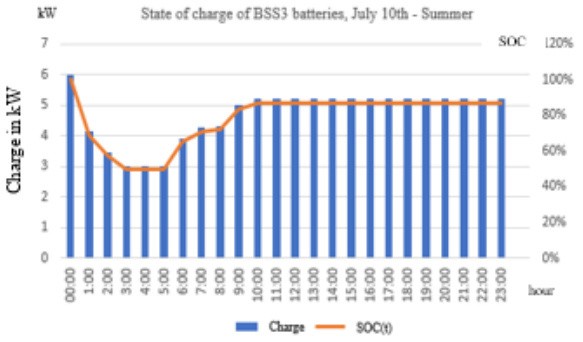

Fig. 11. state of charge of BSS3 batteries, July 10th - Summer

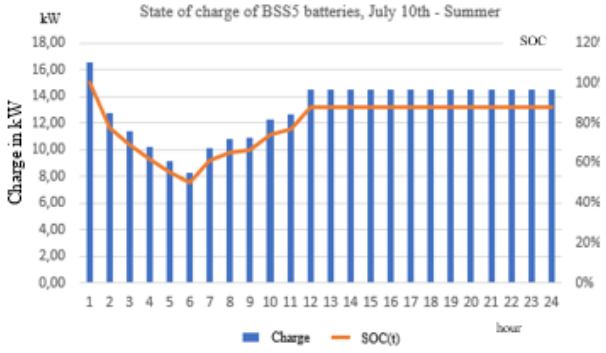

Fig. 12. state of charge of BSS5 batteries, July 10th – Summer.

As shown in Figure 14, the voltage plan was strictly adhered to, and the voltage value did not exceed the regulatory limits for each node at any time of the day.

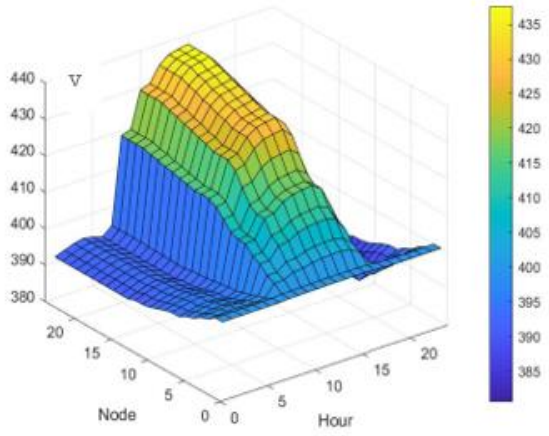

Fig. 13. Voltage (t) in volts at each node of the microgrid over 24 hours, July 10th – Summer.

In the second scenario, the distribution of the contribution from different energy sources is presented in figure 14. Unlike the first scenario, the diesel generator was not utilized throughout the day.

Fig. 14. PSO results, January 21st – Winter.

As shown in Figure 15, the total hourly cost function, incorporating energy prices and greenhouse gas emission taxes, also exhibits two peaks in this scenario. The first peak, reached around 09:00, and the second peak, a global maximum for the day, around 21:00. These two increases in the cost function are explained by the exclusive power supply from the main grid and the load peak also reaching its maximum at these times. The cost function is negative between 14:00 and 17:00 for the same reasons mentioned in the first scenario.

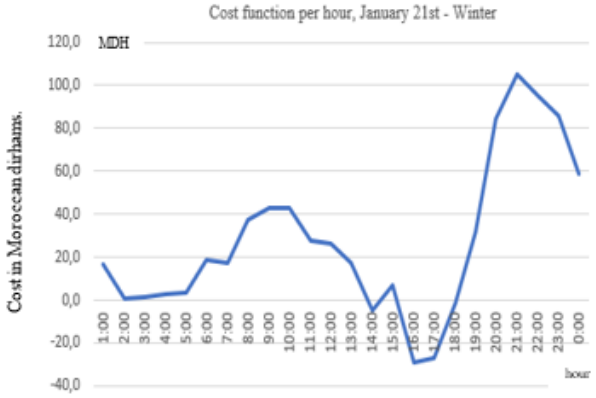

Fig. 15. Cost function per hour, January 21st – Winter.

Similar to the first scenario, greenhouse gas emissions are represented by a curve shown in Figure 16. These emissions peak around 20:00.

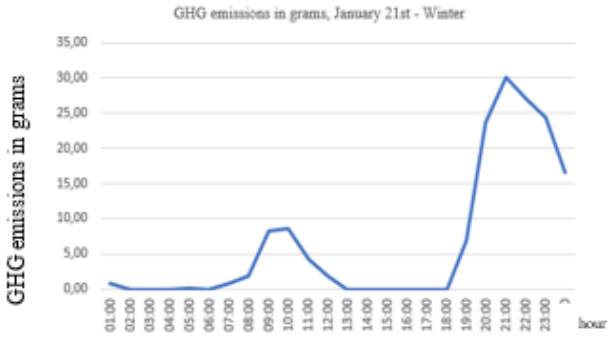

Fig. 16. GHG emission per hour, January 21st – Winter.

Optimization also effectively utilized the energy storage systems (BSSs) in this second scenario. They contributed to powering the microgrid during the night at 01:00 and between 05:00 and 09:00. During this period, photovoltaic energy production from renewable energy sources is at its lowest. The BSSs were charged between 12:00 and 14:00, a period when photovoltaic production is at its maximum.

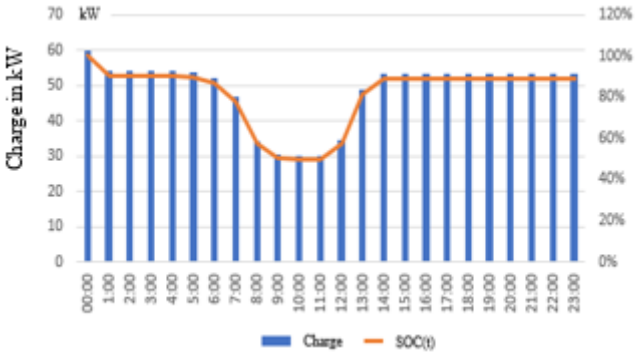

Fig. 17. state of charge of BSS2 batteries, January 21st - Winter

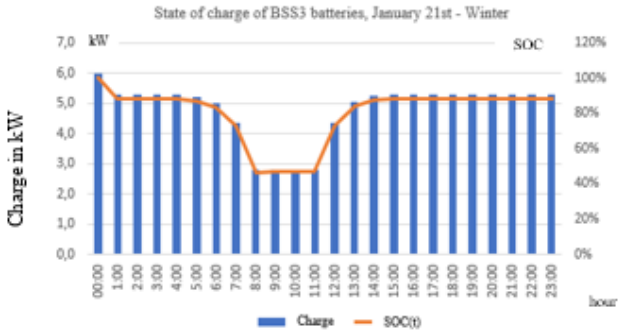

Fig. 18. state of charge of BSS3 batteries, January 21st – Winter.

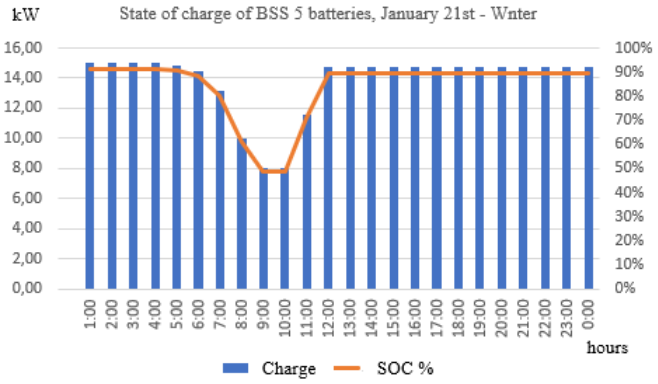

Fig. 19. state of charge of BSS5 batteries, January 21st – Winter.

7. Conclusion

In this study, we have developed an innovative approach aimed at optimizing the management of a microgrid supplying electricity to a rural village, with a particular focus on maintaining the microgrid's voltage profile. Our in-depth analysis of the microgrid's operation has highlighted the effectiveness of the Particle Swarm Optimization (PSO) algorithm in achieving this crucial objective. By integrating the characteristics of various power sources such as wind, photovoltaic, and the diesel generator, we were able to model

the system's behaviour over a day in July and a day in January, considering fluctuations in weather conditions and demand. The obtained results demonstrated that our approach allowed precise and dynamic control of the microgrid's voltage profile. The diesel generator was optimized to intervene strategically during planned outages, minimizing its usage while maintaining the voltage profile within appropriate limits. This optimization reduced costs while ensuring a stable and reliable electrical supply. We have also emphasized the crucial role of battery storage systems in maintaining the voltage profile. They acted as balancers by storing excess energy when available and releasing it when production was insufficient, thus contributing to network stability. In conclusion, this study presents a robust methodology and a successful implementation of the PSO algorithm focused on maintaining the microgrid's voltage profile. The results highlight the crucial importance of this component in ensuring a reliable and high-quality energy supply in microgrids, thereby enhancing their sustainability and operational efficiency.

References

[1] S. Mane, P. Kadam, G. Lahoti, F. Kazi, N.M. Singh, "Optimal load balancing strategy for hybrid energy management system in DC microgrid with PV, fuel cell and battery storage", International Conference on Renewable Energy Research and Applications, (ICRERA), Vol. 5, pp. 1–6, 2016. (Article)

[2] A. Bouakkaz, S. Haddad, J. A. Martín-García, A. J. Gil-Mena, R. Jiménez-Castañeda, "Optimal scheduling of household appliances in off-grid hybrid energy system using PSO algorithm for energy saving", International Journal of Renewable Energy Research (IJRER), Vol.9, No.1, March, 2019. (Article)

[3] P. Cook, "Rural Electrification and Rural Development", London: Springer-Verlag, 1985, ch.2. (Book)

[4] I. F. Tepe and E. Irmak, "A review of control strategies and metaheuristic algorithms used in DC microgrids", International Journal of Renewable Energy Research Vol.12, No.2, June 2022. (Article)

[5] P. V. K. Babu and K. Swarna Sri, "Multi-objective optimal allocation of electric vehicle charging stations in radial distribution system using teaching learning based optimization", International Journal of Renewable Energy Research Vol.10, No.1, March, 2020. (Article)

[6] S. S. Ech-charqaouy, D. Saifaoui, O. Benzohra, A. Lebsir, "Impact of integrating renewable energies into distribution networks on the voltage profile". International Journal of Renewable Energy Research, Vol.10, No.1, March, 2020. (Article)

[7] M. Elsied, A. Oukaour, H. Gualous, R. Hassan. "Gestion de l'énergie et optimisation du système multi-sources basée sur l'algorithme génétique". Symposium de Génie Électrique 2014, Jul 2014, Cachan, France. (Article), ⟨hal-01065314⟩.

[8] https://hal.science/hal-01065314 (consulted 12-02-2023)

[9] S. S. Ech-Charqaouy, D. Saifaoui, O. Benzohra, A. Lebsir, "Integration of decentralized generations into the distribution network - smart grid downstream of the Meter", International Journal of Smart Grid Vol.4, No.1, March, 2020. (Article)

[10] A. A. Moghaddam, "Multi-operation management of a typical micro-grids using particle swarm optimization: A comparative study", Renewable and Sustainable Energy Reviews 16 (2012) 1268– 1281. (Article)

[11] J. Kennedy, R. Eberhart, "Particle swarm optimization", In: IEEE international conf. on neural networks. Piscataway, NJ, vol. 4; 1995. p. 1942e1948. (Article)

[12] A. Anvari-Moghaddam, A. R. Seifi, T Niknam, M. A. Pahlavani, (2011). "Multi-objective operation management of a renewable MG (micro-grid) with back-up micro-turbine/fuel cell/battery hybrid power source". Fuel and Energy Abstracts. 36. 6490-6507. 10.1016/j.energy.2011.09.017.. (Article)

[13] A.Oymak and M. R. Tur, " A Short Review on the Optimization Methods Using for Distributed Generation Planning", Vol.6, No.3, September, 2022, International Journal of Smart Grid. (Article)

[14] R. Eberhart, J. Kennedy. "A new optimizer using particle swarm theory", Sixth International Symposium on Micro Machine and Human Science 0-7803-2676-8/95 – 1995. (Article)

[15] Y. Amoura, A. Pereira, J. Lima, A. Ferreira, H. F. Boukli, A. Kerboua, "Smart Microgrid Management: A Hybrid Optimisation Approach". (2020). 10.21203/rs.3.rs-118351/v1

[16] https://www.researchgate.net/publication/347419322_Smart_Microgrid_Management_A_Hybrid_Optimisation_Approach. (Article) (Consulted 08/01/2023)

[17] Z. B. Nouhou, "Design methodology of a multi-village microgrid", Vol. 2, No. 1, March, 2018 International Journal of Smart Grid,. (Article)

[18] A. M. Elbreki, H. Moria, A. M. Ahmed, M. Elmnifi, A. Abdulmula, "Optimization and performance evaluation of hybrid renewable system for minimizing Co2 emissions in Libya: A case study", International Journal of Renewable Energy Research Vol.10, No.4, December, 2020. (Article)

[19] J. Grimault, "Financer notre stratégie énergie-Climat - donnons-nous les moyens de nos engagements", 2023-004 NOR: CESL1100004X Mercredi 15 février 2023, Copyright © 2023, Conseil Économique Social et Environnemental, CESE. (Article)

[20] https://www.lecese.fr/travaux-publies/financer-notre-strategie-energie-climat-donnons-nous-les-moyens-de-nos-engagements. (Consulted le 10/02/2023).

[21] O. P. Taiwo, R. Tiako and I. E. Davidson, "Voltage profile enhancement in low voltage 11/0.4 kV electric

power distribution network using dynamic voltage restorer under three phase balance load", 2017 IEEE AFRICON, Cape Town, South Africa, 2017, pp. 991-996, ICSMARTGRID. (Article)

[22] M. Ming, R. Wang, Y. Zha, T. Zhang, (2017), "Multi-objective optimization of hybrid renewable energy system using an enhanced multi-objective evolutionary algorithm", Energies, 10(5), 674.

[23] https://doi.org/10.3390/en10050674. (Consulted 02/03/2023)

[24] G. Calas, "Optimisation par essaim particulaire", (SCIA) EPITA 2009. EPITA, 14-16 rue Voltaire, 94270 Le Kremlin-Bicêtre, France. (Article)

[25] F. van den Bergh, "An analysis of particle swarm optimizers", University of Pretoria November 2001, Downloadable in English using the link: https://theses.hal.science/tel-00788961 (consulted 08/01/2023). (Article)

[26] Y. Shi and R. C. Eberhart, "Empirical study of particle swarm optimization," Proceedings of the 1999 Congress on Evolutionary Computation-CEC99 (Cat. No. 99TH8406), Washington, DC, USA, 1999, pp. 1945-1950 Vol. 3, doi: 10.1109/CEC.1999.785511. (Article)

[27] A. El Dor. Perfectionnement des algorithmes d'optimisation par essaim particulaire: applications en segmentation d'images et en électronique. Autre [cs.OH] Université.

[28] https://theses.hal.science/tel-00788961v1, (consulted 05/01/2023) ; (DOCTORAL THESIS)